Floquet analysis of a fractal-spectrum-generating periodically driven quantum system

Rashmi Jangid Sharma,* Tapomoy Guha Sarkar,† and Jayendra N. Bandyopadhyay‡
Department of Physics, Birla Institute of Technology and Science, Pilani 333031, India

(Received 24 April 2018; published 31 October 2018)

We employ Floquet analysis to study the spectral properties of a double-kicked top (DKT) system. This is a classically nonintegrable dynamical system, which also shows chaos. However, even for the underlying classically chaotic dynamics, the quantum quasienergy spectrum of this system does not follow the random matrix conjecture which was proposed for the quantum spectrum of any classically chaotic systems. Instead the quasienergy spectrum of the DKT system shows a butterfly-like self-similar fractal spectrum. Here we investigate the relation between the quasienergy spectrum and the energy spectrum of the corresponding time-independent Floquet Hamiltonian. This Hamiltonian is determined by factorizing the Floquet time-evolution operator into three terms: an initial kick and a final kick, and in between a time-independent evolution dictated by a time-independent Hermitian operator which is called the Floquet Hamiltonian. Like any other generic systems, the Floquet Hamiltonian of the DKT system is also not possible to determine exactly. We apply a recently proposed perturbation theory to obtain the approximate Floquet Hamiltonian at the high-frequency driving limit. We then study the parameter regime where the quasienergy spectrum of the Floquet time-evolution operator matches the energy spectrum of the approximate Floquet Hamiltonian. We have also done a comparative analysis of how the two butterfly spectra disappear with the variation of a system parameter. Finally, we also explore the self-similar property of the energy spectrum of the approximate Floquet Hamiltonian and find its connection with the Farey sequence. Unlike all previous studies, here we have extensively investigated the self-similar property of the whole DKT butterfly.

DOI: 10.1103/PhysRevE.98.042217

I. INTRODUCTION

Hamiltonian systems undergoing periodic delta kicks are studied extensively as a generic model for classical and quantum chaos [1]. This has found new relevance in the possibilities of engineering such systems using ultracold atoms [2–5]. In the traditional approach, such time-dependent systems are theoretically studied by investigating the quasienergy spectrum of the Floquet time-evolution operator. The Floquet time-evolution operator is defined as the time-evolution operator over one period. This quasienergy spectrum contains the imprint of the signature of quantum chaos [1] and quantum criticality with varying parameters of the Hamiltonian [6,7]. Quantum chaos studies have also shown the existence of fractal butterfly patterns in the quasienergy spectrum of some periodically driven systems [8–11], which indicates an infinite number of quantum phase transitions [12]. These systems are particularly interesting because of the fact that, though their classical phase space dynamics may be chaotic, the quantum quasienergy spectrum does not follow the celebrated Bohigas-Giannoni-Schmit (BGS) conjecture [13]. Here we focus on a double-kicked top (DKT) system, which is a prototype model of a classically chaotic system whose quantum spectrum does not follow the BGS conjecture. Two separate kicks within one time period have already been realized in cold atoms in a magneto-optical trap [3]. There is also a possibility of realizing this system in driven two-mode Bose-Einstein condensate systems [14].

We analyze this periodically driven system employing standard Floquet theory. According to this theory, the time-evolution operator of any periodically driven system can be decomposed into a product of three unitary operators. The first and the third unitary operators are called the *micromotion* operators, which describe a time-periodic component of the dynamics. These unitary operators are expressed in terms of Hermitian time-periodic kicked operators which represent the effect of a sudden switching on and off of the time-dependent forcing. The second unitary operator represents a time-independent evolution governed by a time-independent Hermitian operator called the Floquet Hamiltonian or the *effective* time-independent Hamiltonian operator of the periodically driven system. We are investigating spectral properties of the Floquet Hamitonian of the DKT system and comparing its spectrum with the quasienergy spectrum of its corresponding Floquet time-evolution operator.

In most of the physical situations, it is not possible to construct the effective Hamiltonian exactly. Therefore one has to adopt a perturbative technique for its construction. In particular, when the frequency of the driving is large compared to any natural frequency scale of the nondriven problem, then the effective Hamiltonian can be calculated perturbatively with very high accuracy. This happens because the driving cannot resonantly couple with the slower degrees of freedom of the nondriven system. In many situations, the Floquet or effective Hamiltonian is just the time average of

*jangid.rashmi@gmail.com
†tapomoy1@gmail.com
‡jnbandyo@gmail.com

the periodically driven Hamiltonian over a single time period [15]. However, the effective time-independent Hamiltonian of the dynamical system, which we are considering here, is not equal to its time-averaged Hamiltonian. Traditionally, the effective Hamiltonian is obtained from the Floquet time-evolution operator using the Cambell-Baker-Hausdorff (CBH) -based Magnus or Trotter expansion [16]. It has been shown that the CBH-based methods to study the kicked systems suffer intrinsic flaws, and an alternative formulation [17,18] is better suited for more accurate analysis of such systems [7]. The effective Hamiltonian thus obtained is found to mimic the exact time evolution for a large range of parameter values.

This paper begins with a brief discussion on the Floquet formalism and a perturbation scheme to construct an effective static Hamiltonian of a periodically driven system. In Sec. III we introduce the DKT model. Here we discuss the Floquet time-evolution operator of the system and obtain the corresponding effective static Hamiltonian by a perturbation scheme. We also discuss underlying symmetries of the system. In the next section, we discuss the spectral properties of the effective Hamiltonian of the DKT model. Here we show the fractal property of the spectrum and also show the multifractality in the corresponding eigenstates. In Sec. V we show how the DKT butterfly dissolves with the increment of a system parameter. Here we compare this disappearance of the DKT butterfly among its quasienergy spectrum, *unfolded* eigenvalues of its effective Hamiltonian, and eigenvalues of the effective Hamiltonian folded in the first Floquet-Brillouin zone. Section VI discusses the self-similar properties of the DKT butterfly. Here we treated the whole butterfly as a self-similar object and explore this property employing number theoretical approach. Finally, we conclude the paper.

II. FORMALISM

A general time-dependent problem where $\widehat{H}(t) = \widehat{H}_0 + \widehat{V}(t)$, with a time-periodic potential $\widehat{V}(t) = \widehat{V}(t+T)$ of periodicity T, has a Floquet operator $\widehat{\mathcal{F}} = U(T)$ which corresponds to the time-evolution operator for one time period of the external driving. The eigenrelation of the Floquet operator $\widehat{\mathcal{F}}|\phi_\alpha(0)\rangle = \exp(-i\epsilon_\alpha T)|\phi_\alpha(0)\rangle$, where the Floquet modes satisfy the periodic condition $|\phi_\alpha(t)\rangle = |\phi_\alpha(t+T)\rangle$ and ϵ_α are the quasienergies. The quasienergy ϵ_α is not unique; we can always define a quasienergy $\epsilon_{\alpha,n} \equiv \epsilon_\alpha + n\omega$ where $\omega = 2\pi/T$ and n are all integers. This nonuniqueness of the quasienergy is the signature of the temporal periodicity in the Hamiltonian. Here we shall consider the quasienergy spectrum in the first *Floquet-Brillouin* zone, which is defined by $-\omega/2 \leqslant \epsilon_\alpha \leqslant \omega/2$ [19,20].

A traditional approach to extract an effective static Hamiltonian is to write $\widehat{\mathcal{F}} = \exp(-i\widehat{H}_{\rm eff}T)$ and use the CBH expansion to read out $\widehat{H}_{\rm eff}$ up to any order in $T \sim 1/\omega$. This method, however, has been found to suffer from several inadequacies [7,17]. The method used in Refs. [17,18] expresses the time-evolution operator $\widehat{U}(t_i \to t_f)$ between time instants t_i and $t_f = t_i + T$, as a sequence of operations consisting of an initial kick followed by an evolution under a time-independent Hamiltonian and a final "micromotion,"

$$\widehat{U}(t_i \to t_f) = \widehat{\mathcal{U}}^\dagger(t_f) e^{-i\widehat{H}_{\rm eff}T}\,\widehat{\mathcal{U}}(t_i), \tag{1}$$

where $\widehat{\mathcal{U}}(t) = e^{i\widehat{G}(t)}$ such that $\widehat{G}(t) = \widehat{G}(t+T)$ with zero average over one time period. For high-frequency pulsing, the operators $\widehat{H}_{\rm eff}$ and $\widehat{G}(t)$ can be expanded as a perturbation series in $1/\omega$ of the form

$$\widehat{H}_{\rm eff} = \sum_{n=0}^{\infty} \frac{1}{\omega^n}\widehat{H}_{\rm eff}^{(n)}, \quad \widehat{G}(t) = \sum_{n=1}^{\infty} \frac{1}{\omega^n}\widehat{G}^{(n)}. \tag{2}$$

This ansatz along with Eq. (1) can be used to obtain $\widehat{H}_{\rm eff}$ and $\widehat{G}(t)$ up to any desired accuracy. In this method, the average time-independent part is retained in $\widehat{H}_{\rm eff}$, and all the time dependence is pushed to the operator $\widehat{G}(t)$ at each order of perturbation. The convergence of the perturbation series has been surmised in earlier works [17,18]. The periodic potential $\widehat{V}(t)$ may be expanded in a Fourier series as $\widehat{V}(t) = \widehat{V}_0 + \sum_{n=1}^{\infty}(\widehat{V}_n e^{in\omega t} + \widehat{V}_{-n}e^{-in\omega t})$. The truncated series for $\widehat{H}_{\rm eff}$ and $\widehat{G}(t)$ up to $O(1/\omega^2)$ can be expressed in terms of the Fourier coefficients of $\widehat{V}(t)$ [18]. A brief discussion of this method is discussed in Appendix A. We use this as the general expression for the effective Hamiltonian for a system having a periodically *delta function* kicked potential $\widehat{V}(t) = \widehat{V}\sum_n \delta(t - nT)$. The effective Hamiltonian of this system is given by [7,18]

$$\begin{aligned}\widehat{\mathcal{H}}_{\rm eff} &= \widehat{\mathcal{H}}_0 + \frac{\widehat{V}}{T} + \frac{1}{\omega^2 T^2}[[\widehat{V},\widehat{\mathcal{H}}_0],\widehat{V}]\left(\sum_{n=1}^{\infty}\frac{1}{n^2}\right) + O\left(\frac{1}{\omega^3}\right)\\ &= \widehat{\mathcal{H}}_0 + \frac{\widehat{V}}{T} + \frac{1}{24}[[\widehat{V},\widehat{\mathcal{H}}_0],\widehat{V}] + O\left(\frac{1}{\omega^3}\right).\end{aligned} \tag{3}$$

For the simplicity of notation, we would continuously use the notation $\widehat{\mathcal{H}}_{\rm eff}$ to refer the approximate effective time-independent Hamiltonian without explicitly referring to the correction term.

III. MODEL

We are interested in studying the Floquet Hamiltonian of a system whose quasienergy spectrum shows fractal behavior. One such system, which has been studied extensively, is the DKT model [10,11]. The Hamiltonian of this system is

$$\widehat{H} = \frac{2\alpha}{T}\widehat{J}_x + \frac{\eta}{2j}\widehat{J}_z^2 \sum_{n=-\infty}^{+\infty}\left[\delta\left(t - nT + \frac{T}{2}\right) - \delta(t-nT)\right]. \tag{4}$$

The $\widehat{J}_i$ here represent SU(2) generators (angular momentum operators) in the $d = (2j+1)$-dimensional Hilbert space. The time-independent term describes a rotation about x axis of angle α within the time period T. This rotation terms acts all the time on the system. The second term describes a twisting about the z axis of strength η. This term acts stroboscopically and twice within a given period T on the system. However, the direction of the second twisting is the opposite of the first one.

The double kicked systems can be experimentally realized in a cloud of Cs atoms collected in a magneto-optical trap and cooled at the temperature of the order of few micro-Kelvins. The time-dependent potential can be formed by two counter-propagating laser beams incident on the cold atom cloud. This potential is switched on and off by acousto-optic modulators

to create pulses or kicks of pulse width of the order of a few hundreds of nanoseconds [3].

The corresponding time-evolution operator for the given time period $T = 2\pi/\omega$, also known as the Floquet operator, is given as

$$\widehat{\mathcal{F}} = \exp(-i\alpha\widehat{J}_x)\exp\left(-i\frac{\eta}{2j}\widehat{J}_z^2\right)\exp(-i\alpha\widehat{J}_x) \times \exp\left(i\frac{\eta}{2j}\widehat{J}_z^2\right). \quad (5)$$

Following Refs. [10,11], the Floquet operator can be represented in a more compact form as

$$\widehat{\mathcal{F}} = \exp(-i\alpha\widehat{J}_x)\exp\{-i\alpha\widehat{J}_+ e^{i[\eta(2\widehat{J}_z+\mathbb{1})/2j]} + \text{H.c.}\}, \quad (6)$$

where $\widehat{J}_+$ denotes the operator $(\widehat{J}_x + i\widehat{J}_y)/2$. The quasiperiodic nature of the factor $e^{i[\eta(2\widehat{J}_z+\mathbb{1})/2j]}$ for irrational values of the parameter η/j leads to interesting spectral properties [10,11]. The above Floquet operator can also be obtained from a different driven SU(2) Hamiltonian of the form

$$\widehat{\mathcal{H}} = \widehat{\mathcal{H}}_0 + \widehat{\mathcal{V}}\sum_{n=-\infty}^{+\infty}\delta(t-nT), \quad \text{where } \widehat{\mathcal{V}} = \alpha\widehat{J}_x$$
$$\text{and } \widehat{\mathcal{H}}_0 = \alpha\frac{\widehat{J}_+}{T}\exp\left[i\frac{\eta}{2j}(2\widehat{J}_z+\mathbb{1})\right] + \text{H.c.} \quad (7)$$

This is a single kicked system whose Floquet operator, given in Eq. (6), matches exactly with that of the DKT and thereby exhibits interesting Cantor set-like properties in the quasienergy spectrum. Since the double kicked system is now converted into an effective single kicked system, we can now use Eq. (3) to get the Floquet Hamiltonian or the effective Hamiltonian $\widehat{\mathcal{H}}_{\text{eff}}$ approximately up to an order of $1/\omega^2$.

According to the definition, the Floquet modes $|\phi_\alpha(0)\rangle$ are also eigenstates of the Floquet operator $\widehat{\mathcal{H}}_{\text{eff}}$: $\widehat{\mathcal{H}}_{\text{eff}}|\phi_\alpha(0)\rangle = E_\alpha|\phi_\alpha(0)\rangle$. The eigenvalues E_α of $\widehat{\mathcal{H}}_{\text{eff}}$ are just unfolded quasienergies. However, here we have calculated $\widehat{\mathcal{H}}_{\text{eff}}$ approximately up to an order of $1/\omega^2$. Therefore the obtained eigenvalues E_α are the approximate unfolded quasienergies. If we map the unfolded eigenvalues into the first Floquet-Brillouin zone by the transformation $\epsilon_\alpha = E_\alpha \mod \omega$, we shall get the approximate quasienergies up to an accuracy of the order of $1/\omega^2$.

We are interested in the spectral properties of this effective Hamiltonian $\widehat{\mathcal{H}}_{\text{eff}}$. The original time-dependent Hamiltonian $\widehat{H}$ has a unitary symmetry:

$$R_x^\dagger\left(\frac{\pi}{2}\right)\widehat{H}R_x\left(\frac{\pi}{2}\right) = \widehat{H}, \quad \text{where } R_x\left(\frac{\pi}{2}\right) = \exp\left(-i\frac{\pi}{2}J_x\right).$$

For $\alpha/T = \pi/4$, the Hamiltonian $\widehat{H}$ will have an additional unitary symmetry. However, in this paper, we shall mostly consider (except in Sec. VI A) much smaller values of α/T, and therefore this additional symmetry will never appear. This unitary symmetry is also preserved in the effective Hamiltonian $\widehat{\mathcal{H}}_{\text{eff}}$. Because of this symmetry, instead of standard $\{|m\rangle\}$ basis states, we can choose other basis states which are classified as *even* and *odd* basis states [21]:

$$\text{Even: } \left\{|0\rangle,\ \frac{1}{\sqrt{2}}(|2m\rangle + |-2m\rangle),\ \frac{1}{\sqrt{2}}(|2m-1\rangle - |1-2m\rangle)\right\} \text{ of dimension } j+1;$$
$$\text{Odd: } \left\{\frac{1}{\sqrt{2}}(|2m\rangle - |-2m\rangle),\ \frac{1}{\sqrt{2}}(|2m-1\rangle + |1-2m\rangle)\right\} \text{ of dimension } j, \quad (8)$$

where $m = 1, \ldots, j/2$ and we shall always consider j as an even integer. If we write the Hamiltonian $\widehat{\mathcal{H}}_{\text{eff}}$ in the above basis states, the $\widehat{\mathcal{H}}_{\text{eff}}$ matrix will be broken down into a block diagonal form with blocks of size $j+1$ (even block) and j (odd block). These two blocks represent two invariant subspaces of $\widehat{\mathcal{H}}_{\text{eff}}$, and hence they are dynamically independent. Therefore, we can independently study the spectral properties of even and odd subspaces of $\widehat{\mathcal{H}}_{\text{eff}}$, and they are expected to show qualitatively similar behavior. Our numerics have confirmed this fact, and in this paper we are reporting only the results performed for the even subspace. In the even subspace, we denote the basis states as $\{|\overline{m}\rangle\}$, and these are represented in terms of the standard basis states $\{|m\rangle\}$ in the following way:

$$|\overline{m}=0\rangle = |m=0\rangle,$$
$$|\overline{m}\rangle = \frac{1}{\sqrt{2}}(|2m\rangle + |-2m\rangle) \text{ where } \overline{m} = 1, \ldots, j/2 \text{ and } m = 1, \ldots, j/2,$$
$$|\overline{m}\rangle = \frac{1}{\sqrt{2}}(|2m-1\rangle + |1-2m\rangle) \text{ where } \overline{m} = j/2+1, \ldots, j \text{ and } m = 1, \ldots, j/2. \quad (9)$$

IV. RESULTS

A. Properties of the eigenvalues

Figure 1(a) shows the folded energy spectrum of the Hamiltonian $\widehat{\mathcal{H}}_{\text{eff}}$ as a function of $\xi = \eta/2\pi j$ for $\alpha = 1/j$ where we have chosen an even value of spin $j = 20$. We note that odd values of j would bring about changes in the spectrum. The appearance of a butterfly or the static approximate eigenspectrum is in very good agreement with the quasienergy spectrum of the original DKT [10,11]. The spectrum shows qualitative similarity with the Hoftstadter butterfly [22] owing to the presence of the quasiperiodic term. This feature is, however, along the off-diagonal nearest neighbor band and is therefore different from the Harper-Hofstadter case where it appears along the diagonal. In order to study multifractality of the energy spectrum, we set η/j at an irrational value of the

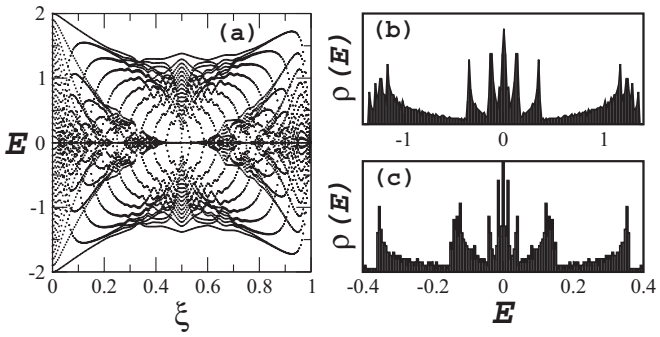

FIG. 1. (a) Energy spectrum of the effective time-independent Hamiltonian of the DKT folded in the first Floquet-Brilouin zone. The spectrum is showing the butterfly pattern. (b)–(c) Self-similarity in the DOS of the energy spectrum is shown by zooming on different scales. Here we set $\xi = G_r/2\pi$, where $G_r = (\sqrt{5}-1)/2$ is the golden mean ratio, the "most irrational number."

golden ratio $G_r = (\sqrt{5}-1)/2$ and a large value of $j = 2500$. To study the statistical property of the energy spectrum, we consider the histogram of eigenvalues for different scales. The density of states (DOS) $\rho(E)$ exhibits self-similarity as seen in Figs. 1(b) and 1(c).

B. Properties of the eigenstates

We have selected *six eigenstates* of $\widehat{\mathcal{H}}_{\text{eff}}$ based on their different (de)localization property as shown in top panel of Fig. 2. We use the participation ratio (PR) as a measure of (de)localization and use that to select the eigenstates. The PR of a state is defined in the following way: If a quantum state of any system $|\Psi\rangle$ is expanded in a (discrete) basis, say, $\{|\phi_m\rangle\}$, then $|\Psi\rangle = \sum_m c_m|\phi_m\rangle$, and the PR of this state in the given basis is $1/\sum_m |c_m|^4$. The PR basically measures how many basis states $\{|\phi_m\rangle\}$ are participating or supporting to construct the given state $|\Psi\rangle$. A larger value of PR means that the state is

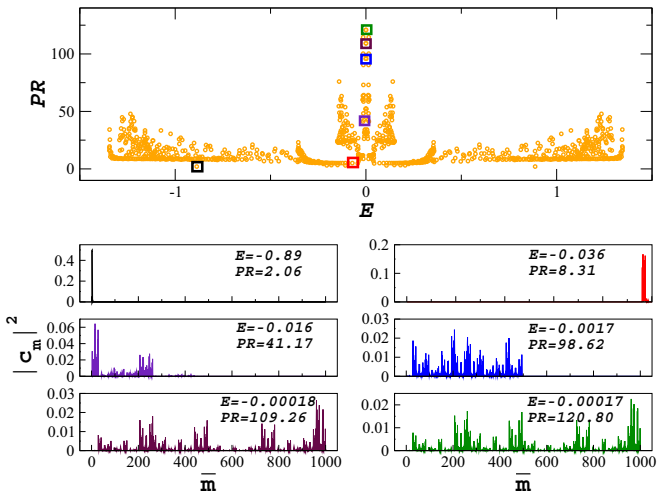

FIG. 2. The top box shows the PR values of all the eigenstates. The remaining six boxes show the selected eigenstates. The energy value and the PR value of these eigenstates are shown.

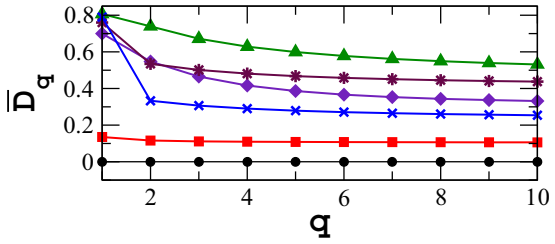

FIG. 3. Generalized fractal dimensions are shown for the above mentioned six eigenstates. The top four states are showing their stronger sensitivity to the scaling parameter q. This indicates their multifractal nature. The remaining two states can be identified as localized states from their PR values. In addition, they also show almost no dependence on q.

highly delocalized, whereas a very small value of PR suggests that the state is localized.

In the top box of Fig. 2 we have plotted the PR values of all the eigenstates. We have selected *six* eigenstates (marked by colored boxes) based on their PR values. The selected eigenstates are presented in the remaining six boxes of Fig. 2. Among the selected eigenstates, one of the eigenstates is very much localized, which has very sharp support over a narrow band of basis states $\{|\overline{m}\rangle\}$ around $\overline{m} = 1$. Its corresponding PR = 2.07, which suggests that approximately *two or three* basis states have a major contribution or support for this state. We have chosen five more eigenstates with PR = 8.31, 41.17, 98.62, 109.26, and 120.80. The PR = 120.80 is the most delocalized state among all the eigenstates of $\widehat{\mathcal{H}}_{\text{eff}}$. Here we have taken $j = 1000$, hence the dimension of the even subspace is $j + 1 = 1001$. Therefore, the PR of the most delocalized eigenstate should be equal to $j + 1 = 1001$, which happens only when all the components of that eigenstate are equal to $1/\sqrt{j+1} = 1/\sqrt{1001}$. However, here we observe that, in comparison to the maximally delocalized state, all the eigenstates of $\widehat{\mathcal{H}}_{\text{eff}}$ are very much localized.

In Fig. 3 we have presented the multifractal property of the selected eigenstates. We study this property by estimating their generalized fractal dimensions $\overline{D}_q$, and these are calculated by the standard box-counting procedure [23]: We consider the components of the nth eigenstate as $\{c_{\overline{m}}^{(n)}\}$ and divide the total dimension $d = j + 1$ into M_l partitions or boxes of linear size $l \sim d/M_l$. We then define the box probability of the eigenstate in the ith box as

$$\widetilde{p}_i(l) = \sum_{\overline{m} \in i\text{'th box}} \left|c_{\overline{m}}^{(n)}\right|^2,$$

where the summation extends over the components $\overline{m}$ in the ith box. We then calculate qth moments of this measure over all boxes and determine $\chi_q(l) = \sum_i \widetilde{p}(i)^q$. For the multifractal eigenstates, it is expected that the measure $\chi_q(l)$ is proportional to some power τ_q of the box size l and τ_q is called the scaling exponent. The generalized fractal dimensions $\overline{D}_q$ are then calculated from the relation $-\tau_q = (q-1)\overline{D}_q = \lim_{l\to 0} \ln \chi_q(l)/\ln l$. According to the definition of $\overline{D}_q$, the parameter q can be any real number. However, here we are restricting ourselves only in the region where $q \geqslant 0$, for the following reason: for the positive values of q, the larger

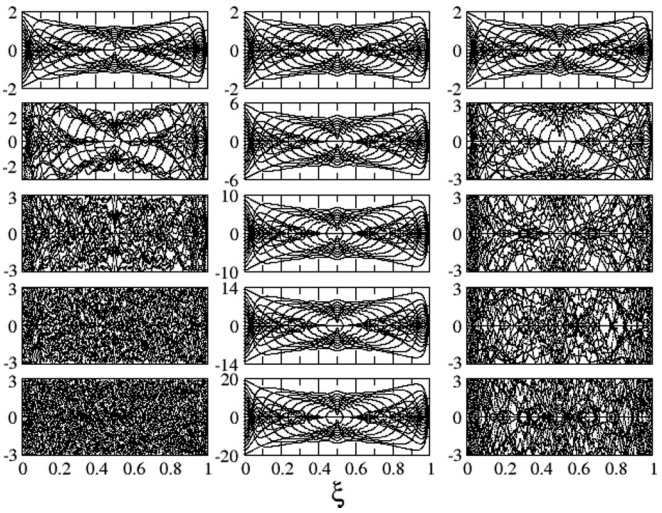

FIG. 4. Disappearance of the DKT butterfly is shown as a function of the parameter $\alpha = n/j$, where $n = 1,\ 3,\ 5,\ 7,\ 10$ (from top to bottom). The left column is showing this behavior in the quasienergy spectrum, whereas the right column is showing the same for the energy spectrum of the Floquet Hamiltonian folded in the first Floquet-Brillouin zone. The central column is showing the unfolded energy spectrum of the Floquet Hamiltonian. At the central column, we do not see any disappearance of the butterfly; however, the size of the butterfly increases with the increment of the parameter α. Here we set $j = 20$.

components of the eigenstates determine $\overline{D}_q$. On the other hand, for the negative values of q, the smaller components of the eigenstates play the major role in determining $\overline{D}_q$. However, the smaller components of the eigenstates are very sensitive to numerical errors, and consequently the calculated values of $\overline{D}_q$ for $q < 0$ will be erroneous.

Figure 3 reveals the following important features of $\overline{D}_q$: According to our expectation, the generalized fractal dimension $\overline{D}_q$ of the most localized state is completely independent of q and $\overline{D}_q = 0$ for all q. The moderately localized state shows very weak q dependence. The other four selected eigenstates show much stronger q dependence on $\overline{D}_q$. Figure 3 also shows a general feature of all the eigenstates: $\overline{D}_q$ is greater for all values of q for the eigenstate with larger PR.

V. DISAPPEARANCE OF THE BUTTERFLY

It is well known for the quasienergy butterfly spectrum of the DKT Floquet operator that it gradually dissolves with the increment of the parameter α [11]. In Fig. 4 we have compared the quasienergy spectrum of $\widehat{\mathcal{F}}$ (left column), the energy spectrum of the effective Hamiltonian $\widehat{\mathcal{H}}_{\rm eff}$ (center column), and the energy spectrum of $\widehat{\mathcal{H}}_{\rm eff}$ folded into the first Floquet-Brillouin zone (right column) for different values of α. The top three boxes are showing these spectra for $\alpha = 1/j$, and they are similar. As we increase the value of the parameter α, we see initial deformation of the butterfly spectrum of the quasienergy spectrum, and eventually it completely disappears at larger values of α. This behavior is already reported in Ref. [11].

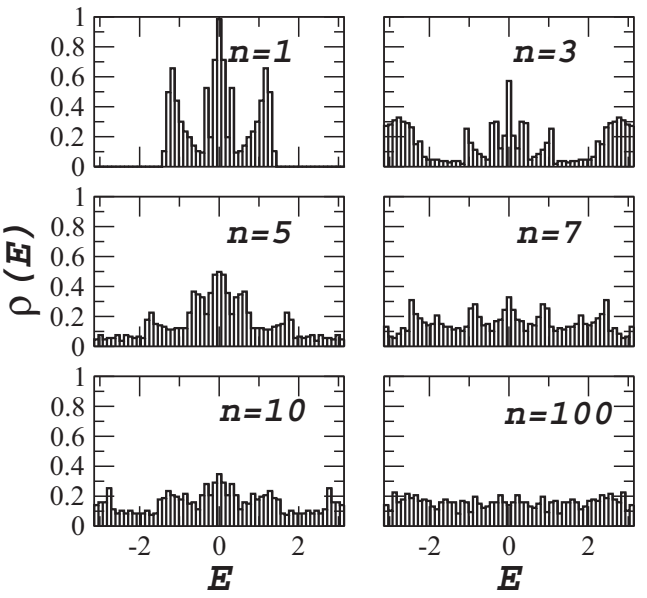

FIG. 5. The DOS of the folded energy eigenvalues of the Floquet Hamiltonian is shown for the same values of the parameter α, which we considered in Fig. 4. In addition, we have also shown the DOS for $\alpha = 100/j$. Here we set the spin size at a very large value $j = 2500$.

At the center column, we have presented the energy spectrum of the effective Hamiltonian $\widehat{\mathcal{H}}_{\rm eff}$ for the same values of α. For this spectrum, we do not see any disappearance of the butterfly, but we observe the enlargement of the butterfly with the increment of α. This behavior is expected because the effective Hamiltonian $\widehat{\mathcal{H}}_{\rm eff}$ up to the order of $1/\omega^2$ has two parts. One part is $\widehat{\mathcal{H}}_0 + \widehat{\mathcal{V}}$, which is linearly dependent on α; and the second part $\frac{1}{24}[[\widehat{\mathcal{V}}, \widehat{\mathcal{H}}_0], \widehat{\mathcal{V}}]$ is quadratically dependent on α. The values of α which we are considering here are very small (order of $1/j$). Therefore, the spectrum of $\widehat{\mathcal{H}}_{\rm eff}$ is mostly dependent linearly on α. Consequently, as we increase α, the size of the butterfly increases linearly with α. Furthermore, if we divide the spectrum corresponding to $\alpha = n/j$ by the factor n, where $n > 1$, then we can project the entire spectrum exactly on the spectrum corresponding to $\alpha = 1/j$. Similarly we can project any two spectrum with different α on the top of each other just dividing or multiplying the spectrum by proper scaling factor. Here we have presented the spectrum for $\alpha = n/j$ where $n = 1,\ 3,\ 5,\ 7,\ 10$, and we set spin $j = 20$.

The energy spectrum of $\widehat{\mathcal{H}}_{\rm eff}$ folded into the first Floquet-Brillouin zone is expected to behave similarly to the quasienergy spectrum. The results presented in the right column of Fig. 4 are indeed showing the dissolution of the folded energy spectrum with the increment of α. However, due to the truncation at $1/\omega^2$, we observe a marginal difference between the quasienergy and the folded spectra for larger $\alpha = n/j$ with $n = 2,\ 5,\ 7$, and 10.

We further study the behavior of DOS $\rho(E)$ of the folded eigenvalues of $\widehat{\mathcal{H}}_{\rm eff}$ as a function of the parameter α for a fixed value of η/j which we set equal to π times the golden mean ratio. Here we set the spin size at very large value $j = 2500$ to get a good statistic for the DOS. In Fig. 5 we have presented $\rho(E)$ for $\alpha = n/j$ where $n = 1,\ 3,\ 5,\ 7,\ 10,\ 100$. The result corresponding to $n = 1$ is already presented in Fig. 1(b). Here

we have presented it again to show the transformation of $\rho(E)$ as a function of α. For $n = 3$, the spectrum has widened to the edge of the first Floquet-Brillouin zone $|E| = \pi$. The central band of the spectrum within $|E| \leqslant 0.4$ still shows the self-similar property. This we have verified by zooming $\rho(E)$ within $|E| \leqslant 0.4$. As we further increase α by varying n, we observe gradual disappearance of the self-similar part of the spectrum around the central band. For a sufficiently large value of α, when $n = 100$, we see a complete disappearance of any self-similarity in the spectrum. Moreover, at this value of α, $\rho(E)$ is approximately flat, which suggests an almost uniform random distribution of the eigenspectrum.

VI. FRACTAL AND SELF-SIMILARITY OF THE DKT SPECTRUM

The best known quantum spectrum which shows a self-similar fractal property is the Hofstadter butterfly. This spectrum was obtained for a system of noninteracting free electrons which are moving in a two-dimensional (2D) surface under the presence of a magnetic field perpendicular to the surface [22]. The butterfly spectrum appears when one plots the energy spectrum as a function of the magnetic flux strength. The fractal properties, as well as the self-similar properties, of the Hofstadter butterfly were mostly studied for some specific values of the magnetic flux strength. Therefore, all these studies were restricted only on some local parts of the butterfly. For the case of the DKT butterfly spectrum, the parameter ξ is playing the role of magnetic flux strength. Also for this butterfly spectrum, all previous studies focused only on some specific parameter values [9–11]. In Sec. IV A we have presented the self-similar properties of the spectrum for a specific value of the parameter $\eta/j = G_r$ or $\xi = G_r/2\pi$, where G_r is the golden ratio. In this section, we study fractal properties and their self-similarity for the whole DKT butterfly spectrum.

A. Fractal properties

In Sec. V we have found that the DKT butterfly spectrum disappears with the increment of the parameter α. This happened in the quasienergy spectrum of the Floquet operator, as well as in the energy spectrum of the perturbatively obtained $\widehat{\mathcal{H}}_{\text{eff}}$. We also observed a complete random distribution of the DOS $\rho(E)$ of $\widehat{\mathcal{H}}_{\text{eff}}$ for very large value of α. We now investigate how the fractal property of the butterfly spectrum obtained from the quasienergy spectrum and the energy spectrum of $\widehat{\mathcal{H}}_{\text{eff}}$ change with parameter α. Here we are assuming that the butterfly is lying on a 2D which is formed by the parameter ξ and the (quasi)energy. We calculate the fractal dimension D_2 of the whole butterfly by the box-counting method [24]. Since the object is lying on a 2D surface, we divide the region into many square boxes or partitions and count the number of points of the butterfly spectrum in each of the boxes. We know the total number of points are used to construct the butterfly from the spin size j and the number of division within the parameter range $0 \leqslant \xi \leqslant 1$. Here we set $j = 20$ and vary the parameter ξ from 0 to 1 in 1000 steps. For the butterfly constructed from the spectrum with even parity, the total number of points is $(j + 1) \times 1000 = 21\,000$. From this, we assign the box probability of individual boxes. We then calculate D_2 as a function of the parameter α and present this result in Fig. 6.

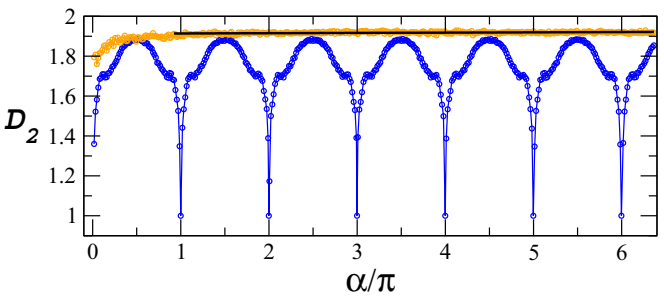

FIG. 6. The whole butterfly is considered as one single fractal object. We have compared how the fractal dimension D_2 varies as a function of the parameter α. Here we have compared this for the butterfly formed by the quasienergy spectrum ϵ (blue circles) and by the folded energy eigenvalues E of the Floquet Hamiltonian (orange circles). The solid black colored straight line is showing how D_2 of the butterfly formed by the folded energy spectrum continuously increasing in linear fashion with slope of the order of 10^{-3} and will reach asymptotically at $D_2 = 2.0$ (Euclidean dimension of the parameter space "$\xi - E$") as a function of α. On the other hand, for the quasienergy spectrum, we see oscillatory behavior of D_2 as a function of α.

We started with $\alpha = 1/j$ where $j = 20$. At this value of α, we observed a nice butterfly in the exact quasienergy spectrum of the Floquet operator and in the energy spectrum of the approximate $\widehat{\mathcal{H}}_{\text{eff}}$. In Fig. 4 we observed that these two butterflies are very much identical, at least to the naked eye. But they are actually not. This fact is revealed while calculating D_2. We have found that D_2 of these two butterflies are not exactly equal for the quasienergy spectrum $D_2 \simeq 1.35$ and for the energy spectrum $D_2 \simeq 1.76$. This indicates some minute differences between these two spectra, which we detect by calculating D_2. In any case, the fractional value of D_2 shows the fractal nature of the DKT butterfly. We then gradually increase the value of the parameter α and observe the variation in D_2. For the quasienergy spectrum (blue line with circles), D_2 reaches its maximum value at $\alpha = \pi/2$, and then D_2 decreases as we increase the parameter α. At $\alpha = \pi$, D_2 goes down to its minima. which is equal to *unity*. We then observe a periodic behavior of D_2 as we increase the value of the parameter α. The fractal dimension D_2 reaches its maxima at $\alpha = (2m + 1)\pi/2$ and its minima $D_2 = 1.0$ for $\alpha = m\pi$, where $m = 0, 1, 2, 3, \ldots$. However, here we have not shown the spectrum for the trivial case of $m = 0$. The periodic behavior of D_2 as a function of α can be understood by substituting $\alpha \to \alpha + m\pi$ in Eq. (5). For any integer value of m, the Floquet operator $\widehat{\mathcal{F}}$ remains invariant. Therefore, the whole quasienergy spectrum within $0 \leqslant \xi \leqslant 1$ will repeat itself for every window of $m\pi \leqslant \alpha \leqslant (m + 1)\pi$. This means that we shall see the identical butterfly for all values of $\alpha = m\pi + 1/j$. The minima $D_2 = 1.0$ is observed for $\alpha = m\pi$ because at these values of α the Floquet operator $\widehat{\mathcal{F}}$ becomes an identity operator. Consequently, in the first Floquet-Brillouin zone, all the quasienergies become degenerate at $\epsilon = 0$ for all values of the parameter ξ. Therefore, the whole quasienergy

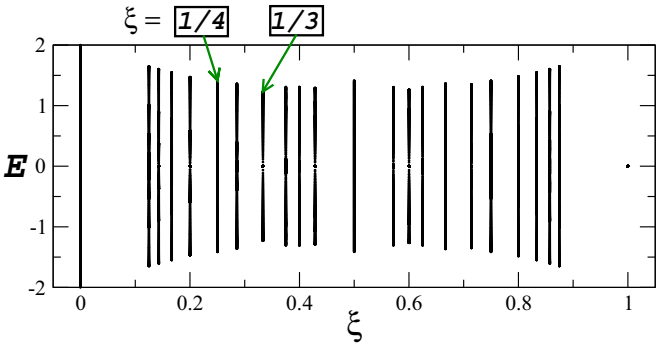

FIG. 7. Skeleton of the DKT butterfly is shown for a set of rational values of the parameter ξ within the range [0, 1]. We have considered those rational numbers which we have obtained from Farey sequence of order 8.

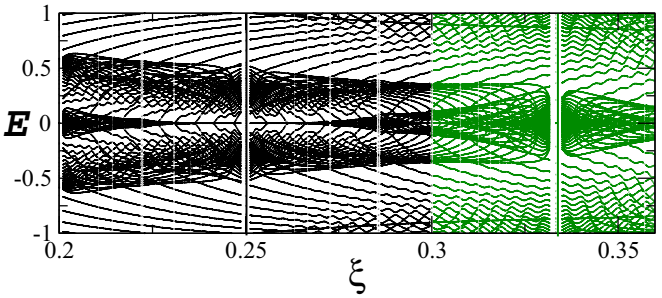

FIG. 8. We have presented the DKT butterfly in the vicinity of two rational values of the parameter ξ: $\xi = 1/4$ (even denominator; black colored region) and $\xi = 1/3$ (odd denominator; green colored region).

spectrum will become a straight line along ξ axis at the energy $E = 0$. For a straight line $D_2 = 1.0$ is expected.

The quantum resonances at $\alpha = m\pi$ are a typical property of the Floquet operator $\widehat{\mathcal{F}}$, and this is not observed in the energy spectrum of $\widehat{\mathcal{H}}_{\text{eff}}$. In Fig. 6 the solid orange line with the circle shows the variation of D_2 as a function of α for the energy spectrum of $\widehat{\mathcal{H}}_{\text{eff}}$. We have given a straight line fitting to this curve in the region $\alpha \gtrsim \pi$. The linear fitting gives a small $O(10^{-3})$ but a positive slope. This suggests a steady increase of D_2 as a function of α, and this will reach asymptotically to a value $D_2 \longrightarrow 2$. This asymptotic value of D_2 is nothing but the Euclidean dimension of the "$\xi - E$ plane" where the whole spectrum is lying.

B. Self-similarity: "Butterfly at every scale"

We now explore self-similar properties of the DKT butterfly using simple geometrical and number theoretical tools. A pattern is called self-similar if it is exactly similar to some part of itself. In other words, if a pattern repeats itself at every scale, then it is called self-similar. Here we analyze the self-similar properties of the DKT butterfly following the method suggested in Ref. [25]. Originally this method was proposed for the analysis of the Hoftstadter butterfly. However, our numeric suggests that the DKT butterfly shares almost similar number theoretical properties with those of the Hofstadter butterfly. However, there is a fundamental difference between these two butterflies. Wings of the Hofstadter butterfly represent gaps in the spectrum. However, we have seen in Fig. 1(a) that the wings of the DKT butterfly are not completely empty, consequently we do not have perfect gaps in the spectrum. Figures 1(b) and 1(c) have shown the absence of any gap in the DOS.

We start our analysis by considering rational values of the parameter ξ. We have constructed these rational values within [0, 1] from Farey sequence [26]. Figure 7 shows a basic structure of the DKT butterfly, which we have obtained using the sequence of rational numbers F_8, the Farey sequence of order 8. This sequence is given in Eq. (B2). In the case of the Hofstadter butterfly, for a fixed rational value of the magnetic flux strength $\phi = \frac{p}{q}$, the energy spectrum has q bands and $(q-1)$ gaps. Moreover, for even values of q, the two central bands of the spectrum touch each other, and therefore $(q-2)$ bands are observed. However, for the DKT butterfly, we do not see such a distinct band gaps for different rational values of the parameter ξ. In Fig. 7 we see continuous spectrum at $\xi = \frac{1}{4}$ (q is even) and $\xi = \frac{1}{3}$ (q is odd). For both these values of q, the Hofstadter spectrum shows *two* gaps. We shall explore more about the gapless property of the DKT butterfly elsewhere [27].

In Fig. 8 we have presented some part of the DKT butterfly. We have shown the behavior of this butterfly in the vicinity of $\xi = \frac{1}{4}$ and $\xi = \frac{1}{3}$. The even denominator fractional value of $\xi = \frac{1}{4}$ forms the center of a butterfly. This is true for every even denominator case. For example, $\xi = \frac{1}{2}$ forms the center of the biggest butterfly. On the other hand, around the odd denominator fractional value of $\xi = \frac{1}{3}$, the behavior of the spectrum is completely different. Here we see a boundary which separates a proliferation of nested butterflies. Unlike the Hofstadter case, here we do not see the left-right symmetry in the spectrum about this boundary at $\xi = \frac{1}{3}$.

We further analyze the "self-similarity" of the DKT butterfly spectrum by studying it at different scales. Here also we closely follow the method proposed in Ref. [25]. As we zoom in the entire butterfly, we obtain butterflies at ever smaller scales, and they exhibit minute details of the original butterfly. We shall refer to the butterflies that are produced on zooming in at different scales as different generations of the DKT butterfly. Each butterfly can be represented by a triplet $(\xi_L = p_L/q_L, \xi_R = p_R/q_R, \xi_C = p_C/q_C)$ of rational numbers, where ξ_L and ξ_R are the left and right edges of the butterflies and $\xi_C = p_C/q_C$ is the center point. The triplets required for the description of butterfly are connected to each other by the relation

$$\frac{p_C}{q_C} = \frac{p_L + p_R}{q_L + q_R} \equiv \frac{p_L}{q_L} \oplus \frac{p_R}{q_R}. \tag{10}$$

The above rule is known as the Farey sum [26]. The different scales of the butterfly can be considered as different generations. The first generation is the full butterfly stretching from $\xi = 0$ to 1. Here we restrict ourselves only to those cases where the larger and the smaller butterflies share neither their left edge nor their right edge. Every generation of the butterfly is obtained by zooming the butterfly in the previous generation. The recursive scheme that connects the two successive

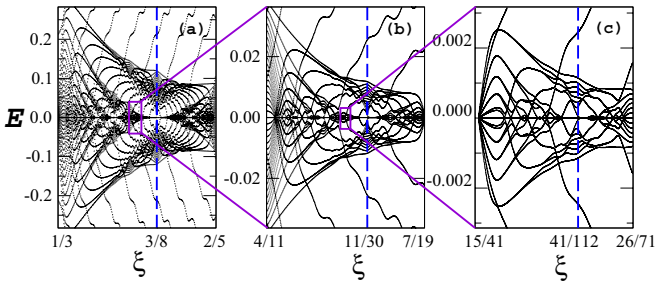

FIG. 9. Self-similarity in the butterfly pattern in the folded energy spectrum of the effective Hamiltonian of the DKT is shown. The ranges of the figures are (a) $\xi = \frac{1}{3}$ to $\xi = \frac{2}{5}$, (b) $\xi = \frac{4}{11}$ to $\xi = \frac{7}{19}$, and (c) $\xi = \frac{15}{41}$ to $\xi = \frac{26}{71}$.

generations of butterfly is given by [25]

$$\begin{aligned}\xi_L(l+1) &= \xi_L(l) + \xi_C(l),\\ \xi_R(l+1) &= \xi_L(l+1) + \xi_C(l),\\ \xi_C(l+1) &= \xi_L(l+1) + \xi_R(l+1),\end{aligned} \tag{11}$$

where l and $l+1$ represents the successive generations.

Figure 9 shows the three successive generations of butterfly. The first generation is shown in Fig. 1(a), whose $\xi_L = \frac{0}{1}$, $\xi_R = \frac{1}{1}$, and $\xi_C = \frac{1}{2}$. This is a complete butterfly. Figure 9(a) shows the second generation of the butterfly. The left and right edges of a second generation butterfly are, respectively, at $\xi_L(l+1) = \frac{0}{1} \oplus \frac{1}{2} = \frac{1}{3}$ and $\xi_R(l+1) = \frac{1}{3} \oplus \frac{1}{2} = \frac{2}{5}$ with its center at $\xi_C(l+1) = \frac{1}{3} \oplus \frac{2}{5} = \frac{3}{8}$. We have obtained these by the above recursion relation given in Eq. (11). Therefore, this second generation butterfly is represented by a triplet $(\frac{1}{3}, \frac{2}{5}, \frac{3}{8})$. Following the above discussed method, we can get butterflies in higher generations. In Figs. 9(b) and 9(c) we have shown, respectively, a third and a fourth generation butterfly. Using the above recursion scheme, we have detected these butterflies, and they are, respectively, represented by the following pair of triplets: $(\frac{4}{11}, \frac{7}{19}, \frac{11}{30})$ and $(\frac{15}{41}, \frac{26}{71}, \frac{41}{112})$. Figure 9 clearly shows that the DKT butterfly is self-similar. Interestingly, we have found that the DKT butterflies share the same Farey sequence-based number theoretical property as that of the Hofstadter butterfly. The two models have no physical similarity whatsoever.

VII. CONCLUSION

In this work we have compared the properties of the quasienergy spectrum of a double kicked top (DKT) system and the energy spectrum of the corresponding static Floquet Hamiltonian. In principle, the Floquet Hamiltonian can be determined by factorizing the Floquet time-evolution operator defined in one single period. However, like any other generic systems, the Floquet Hamiltonian of the DKT system cannot be determined exactly. We have applied a recently proposed perturbation theory to obtain the Floquet Hamiltonian at the limit of high-frequency driving.

The quasienergy spectrum of the periodically driven DKT system gives a butterfly-like self-similar fractal if we plot all the quasienergies as a function of one of the system parameters. If we keep increasing the value of that parameter, then the butterfly spectrum will repeat itself periodically. Since we have obtained the Floquet Hamiltonian approximately by employing a perturbation theory, we have investigated whether the energy spectrum of the Floquet Hamiltonian does share the identical self-similar property. We have found that this is indeed the case if we fold the energy spectrum within the first Floquet-Brillouin zone and consider a certain parameter regime.

In the present work, we have mostly restricted our study within that parameter regime where the quasienergy spectrum and the energy spectrum folded into the first Floquet-Brillouin zone are very much identical. Therefore, we have concentrated mostly on the spectrum of the perturbatively obtained Floquet Hamiltonian. First, we have observed self-similarity in the DOS of the energy spectrum at a parameter fixed at an irrational value. We have also closely looked at the eigenstates and have found a large number of multifractal eigenstates. In addition, we have witnessed many localized eigenstates. The most delocalized eigenstate is also a multifractal state.

Further, we have investigated how the butterfly spectrum can be melted or disappeared by varying a suitable system parameter. For this study, we have compared the quasienergy spectrum of the Floquet time-evolution operator with the energy eigenvalues of the Floquet Hamiltonian for different values of that suitable system parameter. For the energy eigenvalues of the Floquet Hamiltonian, we consider unfolded eigenvalues as well as the eigenvalues folded in the first Brillouin zone. We have observed the disappearance of the butterfly in the quasienergy spectrum and in the folded energy spectrum of the Floquet Hamiltonian. Correspondingly, for the unfolded case, we have not observed any disappearance of the butterfly, but we have observed enhancement of the size of the butterfly without changing its structure.

Finally, we have extensively studied the self-similarity of the butterfly spectrum of the Floquet Hamiltonian. All previous works concentrated on the self-similar property of the DKT butterfly for a particular value of a system parameter. Here we have studied the self-similarity of the whole DKT butterfly as one single object. Following a recent number of theoretical studies of the Hoftstadter butterfly, we have observed identical-looking DKT butterflies in ever smaller scales. Interestingly, we have found that the DKT butterfly shares many of the number theoretical properties with the well-known Hoftstadter butterfly. The reason behind this can be explored in future work.

ACKNOWLEDGMENT

J.N.B and T.G.S, thank DST-SERB, India, for support through Project No. EMR/2016/003289.

APPENDIX A: TIME-INDEPENDENT HAMILTONIAN FOR PERIODICALLY DRIVEN SYSTEM

We consider a general time-dependent Hamiltonian $\widehat{H}(t) = \widehat{H}_0 + \widehat{V}(t)$, with a time-periodic potential $\widehat{V}(t) = \widehat{V}(t+T)$ of periodicity T that has a Floquet operator $\widehat{\mathcal{F}}(t)$ which is the time-evolution operator for one time period. The method used in Refs. [17,18] factors the time-evolution unitary operator $\widehat{U}(t_i \to t_f)$ between times t_i and $t_f = t_i + T$,

as a sequence consisting of an initial kick followed by an evolution under a time-independent Hamiltonian and final kick [18]:

$$\widehat{U}(t_i \to t_f) = \widehat{\mathcal{U}}^{\dagger}(t_f) e^{-i\widehat{H}_{\rm eff}T}\,\widehat{\mathcal{U}}(t_i), \tag{A1}$$

where $\widehat{\mathcal{U}}(t) = e^{i\widehat{G}(t)}$ so that $\widehat{G}(t) = \widehat{G}(t+T)$ with vanishing average over one time period. For high-frequency forcing, the operators $\widehat{H}_{\rm eff}$ and $\widehat{G}(t)$ are expanded as a perturbation series in $1/\omega$ given by

$$\widehat{H}_{\rm eff} = \sum_{n=0}^{\infty} \frac{1}{\omega^n}\widehat{H}_{\rm eff}^{(n)}, \quad \widehat{G}(t) = \sum_{n=1}^{\infty} \frac{1}{\omega^n}\widehat{G}^{(n)}. \tag{A2}$$

This along with Eq. (1) can be used to obtain $\widehat{H}_{\rm eff}$ and $\widehat{G}(t)$ up to any desired order of perturbation. At each order of perturbation, the average time-independent part, in this method, is retained in $\widehat{H}_{\rm eff}$ and all the time dependence pushed to the operator $\widehat{G}(t)$. The convergence of the perturbation series is to be checked on case-by-case basis [17,18]. Expanding the periodic potential $\widehat{V}(t)$ in a Fourier series we have

$$\widehat{V}(t) = \widehat{V}_0 + \sum_{n=1}^{\infty}(\widehat{V}_n e^{in\omega t} + \widehat{V}_{-n}e^{-in\omega t}). \tag{A3}$$

In terms of the Fourier coefficients, the truncated series for $\widehat{H}_{\rm eff}$ and $\widehat{G}(t)$ up to $O(1/\omega^2)$ can be written as

$$\begin{aligned}
\widehat{H}_{\rm eff} &= \widehat{H}_0 + \widehat{V}_0 + \frac{1}{\omega}\sum_{n=1}^{\infty}\frac{1}{n}[\widehat{V}_n, \widehat{V}_{-n}] + \frac{1}{2\omega^2}\sum_{n=1}^{\infty}\frac{1}{n^2}([[\widehat{V}_n, \widehat{H}_0], \widehat{V}_{-n}] + \text{H.c.}) \\
&\quad + \frac{1}{3\omega^2}\sum_{n,m=1}^{\infty}\frac{1}{nm}([\widehat{V}_n, [\widehat{V}_m, \widehat{V}_{-n-m}]] - 2[\widehat{V}_n, [\widehat{V}_{-m}, \widehat{V}_{m-n}]] + \text{H.c.}), \\
\widehat{G}(t) &= \frac{1}{i\omega}\sum_{n=1}^{\infty}\frac{1}{n}(\widehat{V}_n e^{in\omega t} - \widehat{V}_{-n}e^{-in\omega t}) + \frac{1}{i\omega^2}\sum_{n=1}^{\infty}\frac{1}{n^2}([\widehat{V}_n, \widehat{H}_0 + \widehat{V}_0]e^{in\omega t} - \text{H.c.}) \\
&\quad + \frac{1}{2i\omega^2}\sum_{n,m=1}^{\infty}\frac{1}{n(n+m)}([\widehat{V}_n, \widehat{V}_m]e^{i(n+m)\omega t} - \text{H.c.}) + \frac{1}{2i\omega^2}\sum_{n\neq m=1}^{\infty}\frac{1}{n(n-m)}([\widehat{V}_n, \widehat{V}_{-m}]e^{i(n-m)\omega t} - \text{H.c.}).
\end{aligned} \tag{A4}$$

This general expression for the approximate effective static Hamiltonian for periodically driven systems is used in the article.

APPENDIX B: FAREY SEQUENCE

A Farey sequence F_n is the set of rational numbers p/q with p and q, with $0 < p < q < n$, ordered by size. Each Farey sequence start with value 0, denoted by the fraction $\frac{0}{1}$, and ends with the value 1, denoted by the fraction $\frac{1}{1}$. If we have two fractions $\frac{a}{b}$ and $\frac{c}{d}$ with the properties that $\frac{a}{b} < \frac{c}{d}$ and $bc - qd = 1$, then the fractions are known as Farey neighbors, and they appear next to each other in some Farey sequence. The mediant of these two fractions is given by

$$\frac{a}{b} \oplus \frac{c}{d} = \frac{a+c}{b+d}. \tag{B1}$$

The Farey sequences of order 1 to 8 are given as

$$\begin{aligned}
F_1 &= \left\{\frac{0}{1}, \frac{1}{1}\right\} \\
F_2 &= \left\{\frac{0}{1}, \frac{1}{2}, \frac{1}{1}\right\} \\
F_3 &= \left\{\frac{0}{1}, \frac{1}{3}, \frac{1}{2}, \frac{2}{3}, \frac{1}{1}\right\} \\
F_4 &= \left\{\frac{0}{1}, \frac{1}{4}, \frac{1}{3}, \frac{1}{2}, \frac{2}{3}, \frac{3}{4}, \frac{1}{1}\right\} \\
F_5 &= \left\{\frac{0}{1}, \frac{1}{5}, \frac{1}{4}, \frac{1}{3}, \frac{2}{5}, \frac{1}{2}, \frac{3}{5}, \frac{2}{3}, \frac{3}{4}, \frac{4}{5}, \frac{1}{1}\right\} \\
F_6 &= \left\{\frac{0}{1}, \frac{1}{6}, \frac{1}{5}, \frac{1}{4}, \frac{1}{3}, \frac{2}{5}, \frac{1}{2}, \frac{3}{5}, \frac{2}{3}, \frac{3}{4}, \frac{4}{5}, \frac{5}{6}, \frac{1}{1}\right\} \\
F_7 &= \left\{\frac{0}{1}, \frac{1}{7}, \frac{1}{6}, \frac{1}{5}, \frac{1}{4}, \frac{2}{7}, \frac{1}{3}, \frac{2}{5}, \frac{3}{7}, \frac{1}{2}, \frac{4}{7}, \frac{3}{5}, \frac{2}{3}, \frac{5}{7}, \frac{3}{4}, \frac{4}{5}, \frac{5}{6}, \frac{6}{7}, \frac{1}{1}\right\} \\
F_8 &= \left\{\frac{0}{1}, \frac{1}{8}, \frac{1}{7}, \frac{1}{6}, \frac{1}{5}, \frac{1}{4}, \frac{2}{7}, \frac{1}{3}, \frac{3}{8}, \frac{2}{5}, \frac{3}{7}, \frac{1}{2}, \frac{4}{7}, \frac{3}{5}, \frac{5}{8}, \frac{2}{3}, \frac{5}{7}, \frac{3}{4}, \frac{4}{5}, \frac{5}{6}, \frac{6}{7}, \frac{7}{8}, \frac{1}{1}\right\}, \\
&\quad \text{and so on.}
\end{aligned} \tag{B2}$$

[1] H.-J. Stöckman, *Quantum Chaos: An Introduction* (Cambridge University Press, Cambridge, 2007); F. Haake, *Quantum Signatures of Chaos*, 3rd ed. (Springer, Berlin, 2010).

[2] F. L. Moore, J. C. Robinson, C. F. Bharucha, B. Sundaram, and M. G. Raizen, Phys. Rev. Lett. **75**, 4598 (1995); H. Ammann *et al.*, *ibid.* **80**, 4111 (1998); J. Ringot *et al.*, *ibid.* **85**, 2741 (2000); M. B. D'Arcy *et al.*, *ibid.* **87**, 074102 (2001); H. Lignier *et al.*, *ibid.* **95**, 234101 (2005); P. H. Jones *et al.*, *ibid.* **98**, 073002 (2007); J. F. Kanem *et al.*, *ibid.* **98**, 083004 (2007); C. Ryu *et al.*, *ibid.* **96**, 160403 (2006); M. Sadgrove *et al.*, *ibid.* **99**, 043002 (2007); I. Dana *et al.*, *ibid.* **100**, 024103 (2008); G. J. Duffy, S. Parkins, T. Muller, M. Sadgrove, R. Leonhardt, A. C. Wilson, Phys. Rev. E **70**, 056206 (2004).

[3] P. H. Jones, M. M. Stocklin, G. Hur, and T. S. Monteiro, Phys. Rev. Lett. **93**, 223002 (2004).

[4] L. C. Wang, X. P. Li, and C. F. Li, Phys. Rev. B **95**, 104308 (2017).

[5] T. Mishra, A. Pallaprolu, T. Guha Sarkar, and J. N. Bandyopadhyay, Phys. Rev. B **97**, 085405 (2018).

[6] V. M. Bastidas, P. Perez-Fernandez, M. Vogl, and T. Brandes, Phys. Rev. Lett. **112**, 140408 (2014).

[7] J. N. Bandyopadhyay and T. Guha Sarkar, Phys. Rev. E **91**, 032923 (2015).

[8] T. Geisel, R. Ketzmerick, and G. Petschel, Phys. Rev. Lett. **67**, 3635 (1991); R. Ketzmerick, G. Petschel, and T. Geisel, *ibid.* **69**, 695 (1992); R. Artuso *et al.*, *ibid.* **69**, 3302 (1992); R. Artuso, G. Casati, and D. Shepelyansky, *ibid.* **68**, 3826 (1992).

[9] J. Wang and J. Gong, Phys. Rev. A **77**, 031405(R) (2008).

[10] J. Wang and J. Gong, Phys. Rev. Lett. **102**, 244102 (2009).

[11] J. Wang and J. Gong, Phys. Rev. E **81**, 026204 (2010).

[12] N. Goldman, Phys. Rev. A **77**, 053406 (2008); J. Phys. B **42**, 055302 (2009).

[13] O. Bohigas, M. J. Giannoni, and C. Schmit, Phys. Rev. Lett. **52**, 1 (1984).

[14] G. J. Milburn, J. Corney, E. M. Wright, and D. F. Walls, Phys. Rev. A **55**, 4318 (1997); J. Liu, W. Wang, C. Zhang, Q. Niu, and B. Li, *ibid.* **72**, 063623 (2005); Q. Xie and W. Hai, Eur. Phys. J. D **33**, 265 (2005); M. P. Strzys, E. M. Graefe, and H. J. Korsch, New J. Phys. **10**, 013204 (2008).

[15] M. Bukov, L. D'Alessio, and A. Polkovnikov, Adv. Phys. **64**, 139 (2015).

[16] R. Scharf, J. Phys. A **21**, 2007 (1988).

[17] S. Rahav, I. Gilary, and S. Fishman, Phys. Rev. A **68**, 013820 (2003).

[18] N. Goldman and J. Dalibard, Phys. Rev. X **4**, 031027 (2014).

[19] J. H. Shirley, Phys. Rev. **4**, 138 (1965).

[20] H. Sambe, Phys. Rev. A **7**, 2203 (1973).

[21] A. Peres, *Quantum Theory: Concepts and Methods* (Kluwer Academic Publishers, Dordrecht, 2002).

[22] D. R. Hofstadter, Phys. Rev. B **14**, 2239 (1976).

[23] M. Schreiber and H. Grussbach, Phys. Rev. Lett. **67**, 607 (1991).

[24] Almost all books on nonlinear dynamics have discussed about this method. For example see R. C. Hilborn, *Chaos and Nonlinear Dynamics* (Oxford University Press, New York, 1994).

[25] I. Satija, Eur. Phys. J. Spec. Top. **225**, 2533 (2016); I. I. Satija, *Butterfly in the Quantum World* (IOP Publishing, Bristol, 2016).

[26] G. H. Hardy and E. M. Wright, *An Introduction to the Theory of Numbers*, 5th ed. (Oxford University Press, Oxford, 1979).

[27] R. J. Sharma, T. G. Sarkar, and J. N. Bandyopadhyay (unpublished).